PHYSICAL REVIEW E VOLUME 48, NUMBER 6 DECEMBER 1993

Exact renormalization-group approach to the generating function of the Vicsek fractal

J. Q. You,* Chi-Hang Lam,† Franco Nori, and Leonard M. Sander
H. M. Randall Laboratory of Physics, The University of Michigan, Ann Arbor, Michigan 48109-1120
(Received 7 July 1993)

We present an exact real-space renormalization-group approach to study the electronic and vibrational properties of the Vicsek fractal. This approach is developed in the framework of the recursive evaluation of the generating function, which efficiently gives the average density of states (ADOS). The ADOS spectrum consists of hierarchies of isolated peaks following elegant recursive structural rules.

PACS number(s): 64.60.Ht, 63.20.Pw, 71.20.−b, 71.55.Jv

Fractals are ubiquitous in nature and the study of their physical properties is important. In an experiment on a fractal drum, Sapoval *et al.* [1] investigated the transverse vibrations of a membrane bounded by a rigid fractal contour. They observed strongly localized vibrational modes inside fractal cavities, which are connected to the rest of the membrane through narrow paths. Motivated by this experiment, Jayanthi *et al.* examined the vibrations of a Viscek fractal (VF), which has a topology similar to, and much simpler than, the drum with the Koch curve boundary used in the experiment. Using a real-space Green's-function approach, they demonstrated the existence of analogous superlocalized modes in the VF [2]. Here, by means of an exact real-space renormalization-group (RG) technique, we calculate recursively the generating function [3] of the fractal, from which the vibrational and electronic densities of states are computed very efficiently. We are able to obtain the spectra for extremely large system sizes; e.g., the 30th-stage VF, which are already indistinguishable from those of an infinite-size infinite-generation VF [4,5]. The spectra consist entirely of isolated peaks corresponding to highly degenerate superlocalized modes. We found that the peaks are organized in hierarchies following very elegant recursive structural rules. They are more complex than the analogous hierarchies of the Sierpínski gasket [6,7] and the Cantor-set spectra of one-dimensional quasicrystals [8]. Interest in studying the VF, instead of other fractals like the Sierpínski gasket, is enhanced by the fact that the renormalization can be done exactly, and the topology is more similar to the fractal drum studied experimentally by Sapoval *et al.* [1]. In contrast, the Sierpínski gasket has a very different geometry from the drum and has closed loops at all length scales, while the VF fractal has no closed loops.

The VF at the lth stage is composed of $N_l = 5^l$ sites [9]. Figures 1(f) and 1(a) show the first and the second stages, respectively. The generating function is an electronic analog of the partition function used in statistical mechanics and is defined by [3]

$$\mathcal{G}(E) = \frac{1}{N} \ln \left[\int_{-\infty}^{+\infty} \left(\prod_{i=1}^{N} du_i \right) \exp(-\tfrac{1}{2} U^T \underline{X} U) \right]. \quad (1)$$

Here $U = (u_1, u_2, ..., u_N)$, in which N is the number of sites of the system, and the matrix $\underline{X}$ is given by $\underline{X} = Z\underline{I} - \underline{H}$, where $Z = E + i\eta$, $\underline{I}$ is the identity matrix, and $\underline{H}$ the $N \times N$ symmetric Hamiltonian matrix. We consider the one-electron tight-binding Hamiltonian:

$$H = \sum_i | i\rangle \epsilon_i \langle i | + \sum_{i,j} | i\rangle t_{ij} \langle j |, \quad (2)$$

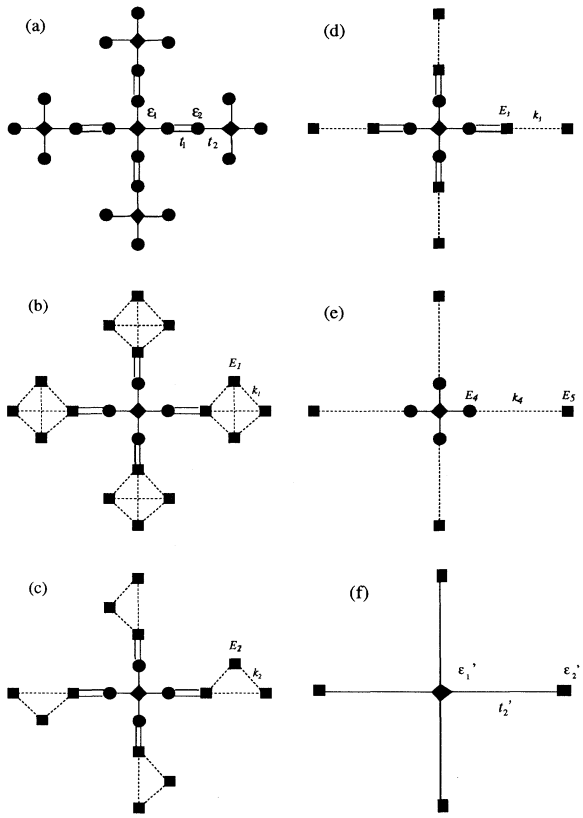

FIG. 1. Schematic illustration of the renormalization-group transformations. (a) A Vicsek fractal at the second stage. (b)–(f) The five decimating substeps which lead to the fractal at its first stage in (f). The initial and the renormalized model parameters are shown in (a) and (b)–(f), respectively.

*Present address: Institute of Modern Physics and Department of Physics, Xiangtan University, Hunan 411105, China.
†Present address: Department of Mathematics, Yale University, New Haven, CT 06520.

where $|\ i\rangle$ is the Wannier state at site i, ϵ_i is the site energy, and t_{ij} the hopping integral associated with the bond connecting sites i and j. The site energy ϵ_i is chosen to be ϵ_1 for the sites with coordination number 4 and ϵ_2 for other sites. We only consider nearest-neighbor interactions and choose t_{ij} to be t_1 for bonds connecting two adjoining two-coordinated sites, and t_2 for the other bonds [see Fig. 1(a)].

For the lth-stage VF, there are N_{l-2} identical subclusters, each of which is a second-stage VF with 25 sites and every two adjoining subclusters are connected by bond t_1. When each of them is decimated to the five-site first-stage VF, the original fractal is transformed to its $(l-1)$th generation. The above step involves simultaneous decimation of several connected sites in every subcluster. The derivation of the RG equations and the evaluation of the integrals in Eq. (1) over the variables associated with the decimated sites become very complicated. Therefore, we sandwich several decimating substeps in between [see Figs. 1(a)–1(f)]. At the first decimating substep, every subcluster of 25 sites in the lth-generation VF, as shown in Fig. 1(a), is converted to the subcluster given in Fig. 1(b). We denote by $\underline{H}_1$ and $\underline{H}_2$ the Hamiltonian matrices corresponding to the decimated and remaining sites, respectively. Then, $U^T\underline{X}U$ can be rewritten as

$$U^T\underline{X}U = U_1^T\underline{X}_{11}U_1 + U_1^T\underline{X}_{12}U_2 + U_2^T\underline{X}_{21}U_1 + U_2^T\underline{X}_{22}U_2 \tag{3}$$

where $\underline{X}_{ii} = Z\underline{I} - \underline{H}_i$, $i = 1,2$, and $\underline{X}_{12} = (\underline{X}_{21})^T$ represents "interactions" between the decimated and remaining sites. Performing the integrals in Eq. (1) over the variables associated with the decimated sites, we have $\mathcal{G}(E) = C' + \mathcal{G}'(E)$ [3,10]. Here C' is a constant given by

$$C' = C + \frac{N_D \ln 2\pi}{2N} - \frac{1}{2N}\ln[\det(\underline{X}_{11})], \tag{4}$$

where $N_D = 4N/5^2$ is the number of decimated sites and det denotes the determinant of a matrix; $\mathcal{G}'(E)$ is the generating function of the system corresponding to the undecimated sites, which is associated with a renormalized matrix

$$\underline{X}'B = \underline{X}_{22} - \underline{X}_{21}(\underline{X}_{11})^{-1}\underline{X}_{12}, \tag{5}$$

where $\underline{X}' = Z\underline{I} - \underline{H}'$ determines the renormalized Hamiltonian of the system corresponding to the undecimated sites.

Since the Hamiltonian matrix $\underline{H}_1$ associated with all the decimated sites is diagonal, it follows from $\underline{X}_{11} = Z\underline{I} - \underline{H}_1$ that the matrix $\underline{X}_{11}$ is also diagonal. Thus, the recursion relation (4) can be explicitly written as

$$C' = C + \frac{N_D \ln 2\pi}{2N} - \frac{N_D}{2N}\ln(Z - \epsilon_1), \tag{6}$$

and from Eq. (5) we obtain the RG equation corresponding to the first decimating substep

$$k_1 = \frac{t_2^2}{Z - \epsilon_1}, \quad E_1 = \epsilon_2 + \frac{t_2^2}{Z - \epsilon_1}, \tag{7}$$

where k_1 is the hopping integral associated with every bond denoted by a dotted line and E_1 the site energy of each site connected by the dotted line in Fig. 1(b). Analogously, similar RG equations are obtained for each of the remaining four decimating substeps [Figs. 1(c)–1(f)]:

$$k_2 = k_1 + k_1^2\gamma_1, \quad E_2 = E_1 + k_1^2\gamma_1, \tag{8}$$

$$k_3 = k_2 + k_2^2\gamma_2, \quad E_3 = E_2 + k_2^2\gamma_2, \tag{9}$$

$$k_4 = t_1 k_3 \gamma_3, \quad E_4 = \epsilon_2 + t_1^2\gamma_3, \quad E_5 = E_3 + k_3^2\gamma_3, \tag{10}$$

$$t_1' = t_1, \quad t_2' = t_2 k_1 \gamma_4, \quad \epsilon_1' = \epsilon_1 + 4t_2^2\gamma_4, \quad \epsilon_2' = E_5 + k_4^2\gamma_4, \tag{11}$$

where $\gamma_i = (Z - E_i)^{-1}$. After the full decimating step, namely from Figs. 1(a) to 1(f), via the intermediate substeps, the generating function can be written as $\mathcal{G}(E) = D' + \mathcal{G}''(E)$. Here, $\mathcal{G}(E)$ and $\mathcal{G}''(E)$ are associated respectively with the Hamiltonian H with parameters ϵ_i and t_i, and the renormalized Hamiltonian H' with parameters ϵ_i' and t_i'. These Hamiltonians have similar forms and correspond to the lth- and $(l-1)$th-generation VF, respectively. The constant D' satisfies the relation

$$D' = D + \frac{2\ln 2\pi}{5} - \frac{2}{5^2}\left[\ln(Z - \epsilon_1) + \sum_{i=1}^{4}\ln(Z - E_i)\right]. \tag{12}$$

For the lth-generation VF with $l \geq 2$, one performs $l-1$ full decimating steps. The RG equations are given by Eqs. (7)–(12) for each of them, except that for the $(l-1)$th full step $t_1' = t_1$ should be removed from Eq. (12), since the VF after this step is converted to an isolated five-site cluster. The generating function of the lth-generation VF is given by

$$D^{(n+1)} = D^{(n)} + \frac{2\ln 2\pi}{5^n} - \frac{2}{5^{n+1}}\left[\ln(Z - \epsilon_1^{(n)}) + \sum_{i=1}^{4}\ln(Z - E_i^{(n)})\right], \tag{13}$$

$$\mathcal{G}(E) = D^{(l)} + \frac{\ln 2\pi}{2\times 5^{l-1}} - \frac{1}{2\times 5^l}\ln[\det(\underline{X}^{(l)})] \tag{14}$$

for $n = 1,2,...,l-1$. Here $\underline{X}^{(l)} = Z\underline{I} - \underline{H}^{(l)}$ and $\underline{H}^{(l)}$ is the renormalized Hamiltonian matrix of the isolated five-site cluster. The determinant of $\underline{X}^{(l)}$ is

$$X = (Z - \epsilon_2^{(l)})^3[(Z - \epsilon_1^{(l)})(Z - \epsilon_2^{(l)}) - 4(t_2^{(l)})^2]. \tag{15}$$

The initial condition for Eq. (13) is $D^{(1)} = 0$, $\epsilon_1^{(1)} = \epsilon_1$, and $E_i^{(1)} = E_i$, $i = 1$ to 4.

The average density of states (ADOS) is given by [3]

$$\rho(E) = \frac{2}{\pi} \lim_{\eta \to 0} \mathrm{Im} \frac{\partial \mathcal{G}}{\partial E}, \tag{16}$$

where Im denotes the imaginary part of a complex quantity. Contrary to the generating function defined by Lemieux *et al.* [3], Eq. (1) contains a factor $1/N$. Thus, Eq. (16) gives the density of states divided by N, namely the ADOS. From Eqs. (13), (14), and (16), we obtain the ADOS of the lth-generation structure

$$\rho(E) = \frac{1}{\pi} \lim_{\eta \to 0} \mathrm{Im} \left\{ \frac{1}{5^l} \left(\frac{Y}{X} \right) + \sum_{n=1}^{l-1} \frac{4}{5^{n+1}} \left[\frac{p_0^{(n)}}{Z - \epsilon_1^{(n)}} + \sum_{i=1}^{4} \frac{p_i^{(n)}}{Z - E_i^{(n)}} \right] \right\}, \tag{17}$$

where $Y = \partial X / \partial Z$, $p_0^{(n)} = 1 - \partial \epsilon_1^{(n)} / \partial Z$, and $p_i^{(n)} = 1 - \partial E_i^{(n)} / \partial Z$, $i = 1$ to 4.

The transverse vibrations of the fractal are described by the equation of motion $-m\omega^2 \psi_i = \sum_{j \neq i} K_{ij} (\psi_j - \psi_i)$, where ψ_i is the displacement perpendicular to the fractal plane of mass m placed at site i, and K_{ij} is the spring constant between sites i and j. We choose K_{ij} to be K_1 and K_2 for the bonds denoted by double and single solid lines, respectively, in Fig. 1(a). Each of the boundary sites is anchored by spring constant K_1 to a rigid boundary [2]. The equation of motion can be recast in the form similar to the electronic Hamiltonian in Eq. (2). The parameters are related by $\epsilon_1 = 4K_2/m$, $\epsilon_2 = (K_1 + K_2)/m$, $t_1 = -K_1/m$, and $t_2 = -K_2/m$, while E is replaced by ω^2. Using the RG technique, we also calculated the vibrational ADOS.

Figures 2(a) and 2(b) present, respectively, the electronic and vibrational ADOS's of the VF at its 30th stage, where we choose $\epsilon_1 = \epsilon_2 = 0$, $t_1 = t_2 = 1$, and $K_1/m = K_2/m = 1$, respectively. We take $\eta = 10^{-3}$ to approximate the limit $\eta \to 0$ in Eq. (17). The ADOS's exhibit hierarchical structures composed of isolated peaks. If a smaller η is taken, every peak becomes sharper and more structures become visible. Each peak corresponds to a highly degenerate state. The high degeneracies result from the rich symmetry of the system. For the first-stage fractal, the Hamiltonian is invariant under the permutation of the four outer sites. The second generation consists of four sidebranches, each of six sites, connected to the central atom. The symmetry operations include the permutation of the four sidebranches and also the permutation of the three outer sites in each sidebranch. In general, the symmetry group of the lth-stage VF with nearest-neighbor interactions is a direct product of permutation groups. This symmetry is much richer than, for example, the point groups for usual molecules.

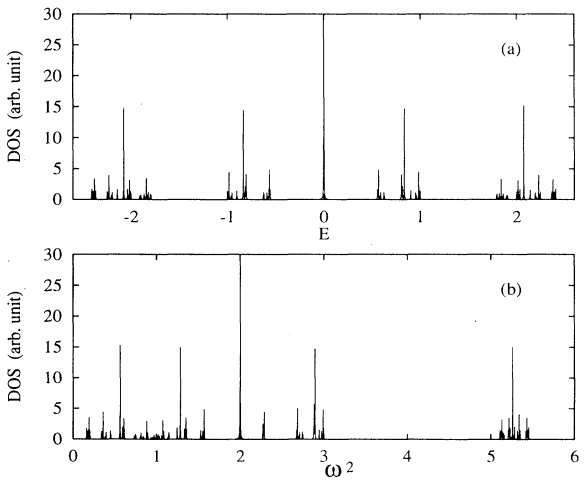

FIG. 2. Average DOS (arbitrary units) of the Vicsek fractal: (a) electronic DOS for $\epsilon_1 = \epsilon_2 = 0$ and $t_1 = t_2 = 1$ (in units of t_1); (b) vibrational DOS, where $K_1/m = K_2/m = 1$ (in units of K_1/m).

By examining the nature of the normal modes as dictated by the symmetry, the degeneracy of all the modes can be obtained by means of systematic counting. The details will be reported elsewhere. Here we summarize those results relevant to the interpretation of the ADOS's. The spectra consist completely of isolated peaks of various degeneracies. The total number of peaks at the lth stage is proportional to $(2 + \sqrt{3})^l$ asymptotically, much less than the number of sites N_l. A constant fraction of them correspond to nondegenerate modes and make a vanishing contribution to the ADOS at large l. The ADOS's are dominated only by the highly degenerate modes. We group the peaks into sets according to the degeneracies. The first set contains only one peak at $\omega^2 = 2$. It has the highest degeneracy per site, which can be shown to be exactly 6/25. The second set consists of the four peaks having the second highest degeneracy per site of 6/125. In general, the ith set has p_i peaks of degeneracy $6/5^{i+1}$, where p_i is given by $p_i = 4p_{i-1} - p_{i-2}$. All these exact results agree well with the ADOS in Fig. 2. Apparent nonuniformity of the peak heights for the third and the higher sets are due to adopting a finite η in Eq. (17).

The hierarchical structures result from the self-similarity of the fractal. We first examine Fig. 3(a), which shows the electronic ADOS with parameters $\epsilon_1 = 1$, $\epsilon_2 = 0$, $t_1 = t_2 = 1$. The spectrum is composed of one highest peak and four clusters containing the four second highest peaks. Figures 3(b) and 3(c) expand the first and the second clusters on the left respectively, where $\eta = 10^{-4}$ is taken. We denote the clusters by the second level structures and the original one by the root structure. They are similar to each other but not identical. The hierarchies in Figs. 3(b) and 3(c) are the two stabilized structures characterizing the tree. Upon further magnification, these two structures and their mirror images reappear recursively. Let us refer to the structures as types A and B, respectively, and the mirror images by A' and B'. In general, structure A [Fig. 3(b)] at the ith level is composed of a main isolated peak belonging to the ith set (according to the above classification by degeneracy) sandwiched between four smaller structures of the $(i+1)$th level. The four structures, starting from

the left, are of type A, A', B', and A, respectively. This recurrence in magnifying from the ith to the $(i+1)$th level can be summarized by the recursive structural rule: $A \rightarrow AA'IB'A$, where I denotes the main isolated peak. Structure B [Fig. 3(c)] has only three subclusters and the recursive rule is $B \rightarrow A'IB'A$. The rules for the mirror images follow trivially.

The precise structure at the root level depends on the model parameters. For Figs. 3(a) and 2(b), the composition is $ABIAA'$, but the structures A and B on the left overlap each other. We can interpolate between Figs. 3(a) and 2(a) by decreasing ϵ_1 from 1 to 0. The third level structure of type A' at $E \simeq 0.15$ in Fig. 3(a) merges with the first level isolated peak at $E = 0$ in Fig. 2(a). The root structure thus becomes $ABIB'A'$, where the degeneracy of the main peak is enhanced. For this set of parameters, the spectral structure is symmetrical with respect to the $E = 0$ axis due to additional symmetry. In some cases, there exist anomalies in the ordering of the subclusters, especially at levels close to the root. For example, the peak I and the structure B' in the recursive rule of A is sometimes interchanged. At increasingly high magnification, inside a structure of type A, the width of its substructure B' and its distance from I decrease relatively. Asymptotically, the substructure B' collapses into I to form a single peak.

The spectrum of the Sierpínski gasket was computed exactly by Rammal using a similar generating function method [7], and by Domany *et al.* directly from the recursion relation for the energy renormalization [6]. The Sierpínski gasket spectrum has analogous but simpler self-similar properties; e.g., there is only one type of substructure, in contrast to the two types, A and B, for the VF. This is because, for the Sierpínski gasket, the sites decimated in each step are equivalent, and the recursion relation has a simple quadratic form. However, for the VF case, there are five different substeps. The overall recursion relations for the full step obtained by combining Eqs. (7)–(12) are substantially more complicated. The complexity of the relations leads to the much richer properties of the hierarchies.

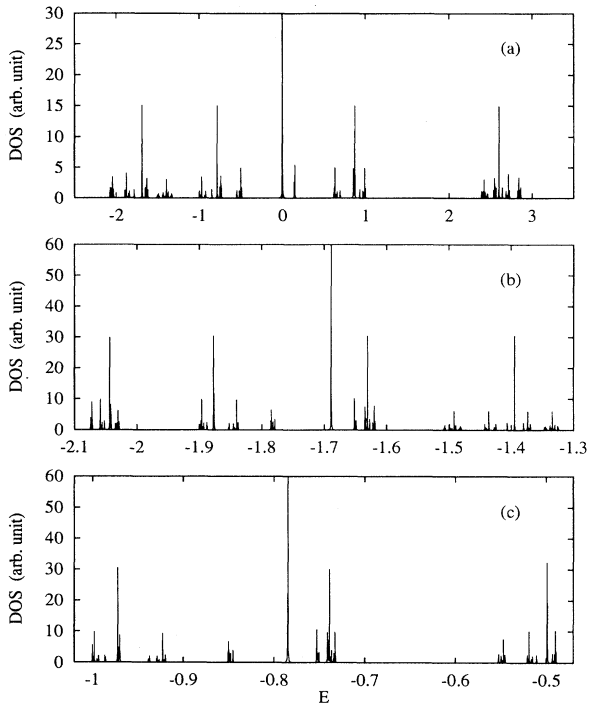

FIG. 3. Average electronic DOS (arbitrary units) of the Vicsek fractal for $\epsilon_1 = 1$, $\epsilon_2 = 0$, $t_1 = t_2 = 1$ (in units of t_1): (a) shows the complete spectrum; (b) and (c) show magnifications of the first and the second subclusters on the left, respectively.

J.Q.Y. is supported by the National Natural Science Foundation of China and he thanks the Physics Department of the University of Michigan for hospitality. C.-H.L. and L.M.S. are supported by NSF Grant No. DMR91-17249. F.N. acknowledges partial support from a GE fellowship, a Rackham grant, and SUN microsystems.

[1] B. Sapoval, Th. Cobron, and A. Margolina, Phys. Rev. Lett. **67**, 2974 (1991).

[2] C.S. Jayanthi, S.Y. Wu, and J. Cocks, Phys. Rev. Lett. **69**, 1955 (1992).

[3] M.-A. Lemieux and A.-M.S. Tremblay, Phys. Rev. B **36**, 1463 (1987); M.-A. Lemieux, P. Breton, and A.-M.S. Tremblay, J. Phys. (Paris) Lett. **46**, L1 (1985).

[4] After we completed our main computation, C.S. Jayanthi kindly sent us copies of work of an exact calculation of the phonon frequency spectrum for the VF of a similar size, obtained by solving algebraic equations that follow from an explicit examination of the dynamical matrix [5]. Their result agrees with our Fig. 2(b).

[5] C.S. Jayanthi and S.Y. Wu (unpublished).

[6] E. Domany, S. Alexander, D. Bensimon, and L.P. Kadanoff, Phys. Rev B **28**, 3110 (1983).

[7] R. Rammal, J. Phys. (Paris) **45**, 191 (1984).

[8] Q. Niu and F. Nori, Phys. Rev. B **42**, 10 329 (1990).

[9] See, e.g., L.M. Sander, Sci. Am. **256**(1), 94 (1987).

[10] J.A. Ashraff and R.B. Stinchcombe, Phys. Rev. B **39**, 2670 (1989).